Korean J. Chem. Eng., 33(1), 178-188 (2016)
DOI: 10.1007/s11814-015-0106-y

pISSN: 0256-1115
eISSN: 1975-7220

Ultrasound-assisted adsorption of textile dyes using modified nanoclay: Central composite design optimization

Aydin Hassani*, Reza Darvishi Cheshmeh Soltani, Murat Kıranşan*, Semra Karaca*,†, Canan Karaca*, and Alireza Khataee***,†**

*Department of Chemistry, Faculty of Science, Atatürk University, 25240 Erzurum, Turkey
**Department of Environmental Health Engineering, School of Health,
Arak University of Medical Sciences, 38196-93345 Arak, Iran
***Research Laboratory of Advanced Water and Wastewater Treatment Processes,
Department of Applied Chemistry, Faculty of Chemistry, University of Tabriz, 51666-16471, Tabriz, Iran
(*Received 17 January 2015 • accepted 16 May 2015*)

Abstract−The removal of two anionic dyes, C.I. Acid Orange 7 (AO7) and C.I. Acid Red 17 (AR17), by ultrasound-assisted adsorption on the modified nanoclay in aqueous solutions was studied. The modified nanoclay was characterized by SEM/EDX, BET, XRD and FT-IR techniques. The average crystal size for the interlayer spacing of the modified nanoclay was about 14.3 nm. Central composite design (CCD) was used for the optimization of the operational parameters, including the initial dye concentration, sonication time, adsorbent dosage and temperature. The results demonstrated a good agreement between the predicted values obtained by the model and the experimental values for both AO7 (R^2= 0.959) and AR17 (R^2=0.971).

Keywords: Anionic Dyes, Experimental Design, Nanoclay, Sono-adsorption

INTRODUCTION

Discharging colored wastewater into water resources leads to detrimental effects on the environment, potential risk to human health, toxicity to flora and fauna and derogatory effects on the photosynthesis [1-4]. Therefore, the purification of colored wastewaters has become an extremely important topic [5,6]. Among available treatment techniques used for dye removal, such as coagulation and flocculation, membrane filtration, ozonation, and biological processes [1-3,5,6], the adsorption process has proven to be effective and reliable for removing dyes from aqueous solutions [7-11]. The adsorption process has ease of operation, cost efficiency, availability of adsorbents and no sludge formation [1-3,5,6,12,13]. However, the application of activated carbon as the most widely used adsorbent has decreased due to its high operational and capital costs, the necessity of regeneration and the reduction of activity after regeneration [7,14]. There is a growing demand to develop new adsorbents for the decolorization of aqueous solutions. Natural clays have been considered as environmentally friendly, cheap, abundant and ion exchangeable adsorbents [9,15-17]. Montmorillonite, as one of the most widely used clay materials, is a promising alternative to activated carbon because it is available, relatively cheap (its natural form), easily extracted, non-toxic and mechanically and chemically stable [9,18]. However, the application of pristine montmorillonite is not efficient enough for removing anionic pollutants from aqueous media, because its negatively charged surface leads to repelling the negatively charged contaminants. For this reason, to extend the use of clays in anionic contaminant-contained solutions, modified clays with a suitable chemical agent are preferred to the natural clays [9]. In the present study, commercial montmorillonite clay modified by dimethyl dialkyl amine has been used as a new adsorbent to increase its capacity for removing two organic dyes. Recently, to cope with the limitations of other processes, such as high cost, ineffectiveness for the removal of some pollutants, operation problems and production of toxic secondary pollutants, adsorption combined with other processes for wastewater treatment has been accepted as an effective purification process to reduce the traces of organic pollutants. One of the innovative technologies used in combination with adsorption is sonication. In addition, it has been demonstrated that the removal efficiency can be improved by the combination of ultrasonication and adsorption processes due to the disadvantages of the application of adsorption alone such as high cost, ineffectiveness for the removal of some pollutants, operation problems and production of toxic secondary pollutants [19]. Ultrasound radiation accelerates chemical processes due to acoustic cavitation (i.e., the formation, growth and collapse of micrometrical bubbles). The ultrasound waves enhance the mass and heat transfer rate at interfacial films surrounding the adsorbent surface [19,20]. Although most organic compounds can be decomposed by the ultrasound irradiation, the decomposition rates are still slow for practical uses. To enhance the decomposition rate, the addition of solid particles or reagents is one of the suggested methods [2,19,20]. Thus, degradation of the organic pollut-

†To whom correspondence should be addressed.
E-mail: a_khataee@tabrizu.ac.ir, ar_khataee@yahoo.com, skaraca@atauni.edu.tr, semra_karaca@yahoo.com

ants is carried out in shorter time and, consequently, the required time, energy and cost are reduced. The main aim of the present work was the adsorption of two anionic dyes, C.I. Acid Orange 7 (AO7) and C.I. Acid Red 17 (AR17), in the aqueous phase using modified montmorillonite nanoclay as the adsorbent. In the following, the effect of the ultrasound radiation on the amount of the adsorbed organic dye has been evaluated. To vigorously evaluate the effect of various operational parameters, including the initial dye concentration, sonication time, adsorbent dosage and temperature, on the adsorption of AO7 and AR17 via ultrasound-assisted adsorption, response surface methodology (RSM) based on central composite design (CCD) were employed [21]. RSM is used to determine the efficiency of an experimental system [22-24]. By using RSM, various parameters are simultaneously examined with a minimum number of experiments, thereby indicating that the study processed by RSM can be less expensive and time consuming in comparison with the conventional one-factor-at-a-time statistical strategy [23,25,26].

MATERIALS AND METHODS

1. Chemicals

The montmorillonite clay modified with 35-45 wt% dimethyl dialkyl amine was purchased from Sigma Aldrich Co. and used as the adsorbent with a zeta potential value of +74.5 mV. All chemicals and reagents, which were of analytical grade, were purchased from Merck, Germany. Organic anionic dyes (AO7 and AR17) were purchased from Shimi Boyakhsaz Company, Iran, and used as received. The specifications of the purchased dyes are given in Table 1.

2. Ultrasound-assisted Multi-component Adsorption of AO7 and AR17 onto Nanoclay

Batch reactors were used to conduct the experiments of ultrasound-assisted adsorption using the modified nanoclay in the presence of ultrasound radiation. All experiments were in a round-bottom glass flask by adding a known amount of the adsorbent to 100 mL solution of (20-60 mg/L) AO7 and AR17 at the initial pH of the solution, which was the natural pH of the dyes (5.70 for AO7 and 5.85 for AR17). The vessel was immersed in an ultrasonic bath with temperature control. In the experiments, the initial dye concentration, adsorbent dosage, temperature and sonication time were in the range of 20-60 mg/L, 0.45-0.85 g/L, 20-40 °C and 4-20 min in a 640 W ultrasonic bath (Bandelin Sonorex, Germany), respectively. For the adsorption experiments in a stagnant medium (without ultrasound radiation), 0.65 g and 0.54 g of modified nanoclay were added to 100 mL of the pollutant solution with the desired initial concentration of AR17 and AO7, respectively. The mixture was kept under agitation at 150 rpm in a temperature controlled shaker (Julabo SW22, Germany). Then it was analyzed to determine color removal (%).

3. Analysis

At the end of the experimental runs of adsorption or ultrasound-assisted adsorption, a 5 mL sample was withdrawn and immediately centrifuged for 5 min at 6,000 rpm to determine the residual concentration of AO7 and AR17 dyes via a Varian UV-visible spectrophotometer (Model: Cary 100, Australia) at 485 and 514 nm, respectively. The removed amount of dye was calculated from the difference between the concentrations in the solution before and after adsorption. The dye removal efficiency was calculated by using Eq. (1):

$$\text{Color removal}\ (\%) = \frac{(C_0 - C_t)}{C_0} \times 100 \tag{1}$$

where C_0 (mg/L) and C_t (mg/L) refer to the concentration of the dyes at the beginning and time t, respectively. The amount of the adsorbed dye (q) as mg/g was calculated via Eq. (2):

$$q = \frac{(C_0 - C_e) \times V}{M} \tag{2}$$

where C_0 (mg/L) and C_e (mg/L) are the initial and equilibrium concentrations of the dye, respectively. Moreover, V (L) is the volume of the solution and M (g) is the mass of the adsorbent. Brunauer-Emmett-Teller (BET) analysis determined the specific surface area of the adsorbent by means of a nitrogen adsorption-desorption isotherm measured at 77 K in some relative pressure ranging from 0.05 to 0.4 (Belsorp mini II Bel, Japan). Barret-Joyner-Halender (BJH) method was used to obtain pore size distribution [27]. Prior to measurement, the sample was degassed at 100 °C for 15 h in the degas port of the analyzer. Scanning electron microscopy (SEM) was conducted on a Philips scanning electron microscope (XL 30 SFEG, the Netherlands) to evaluate the surface morphology of the

Table 1. Characteristics of C.I. Acid Orang 7 and C.I. Acid Red 17

C.I. name	Chemical structure	Molecular formula	M_w (g/mol)	λ_{max} (nm)	Class
Acid orange 7 (AO7)	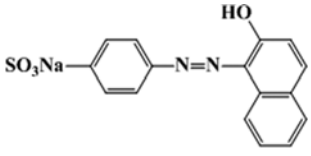	$C_{16}H_{11}N_2NaO_4S$	350.32	485	Monoazo
Acid red 17 (AR17)	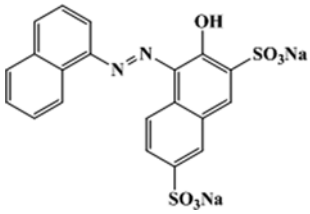	$C_{20}H_{12}N_2Na_2O_7S_2$	502.43	514	Monoazo

adsorbent. To ensure the purity, presence and distribution of specific elements in a solid sample, SEM images were further supported by the energy dispersive X-ray (EDX) microanalysis. Fourier transform infrared (FT-IR) spectra of the as-prepared samples before and after the adsorption of the dyes were taken in the wavenumber range of 400-4,000 cm^{-1} using a Perkin Elmer spectrometer (Model: 1600, USA). The X-ray diffraction (XRD) pattern of the nanoclay was obtained by a Philips X-ray diffractometer (XRD, STOE D-64295, Germany). The zeta potential of the modified nanoclay/water suspension was measured using Zeta-Meter 3.0+, Inc., Staunton, VA, USA.

4. Experimental Design

Four main parameters (the initial dye concentration (mg/L) (X_1), sonication time (min) (X_2), adsorbent dosage (g/L) (X_3), and temperature (°C) (X_4)) influencing the adsorption of anionic organic dyes onto the nanoclay, were chosen for the experimental design via CCD. According to the CCD model, the number of experimental runs was calculated with Eq. (3):

$$N=2^k+2k+x_0 \quad (3)$$

where N, k and x_0 are the number of the experimental runs, the number of parameters and the number of central points, respectively [17,18]. Accordingly, the total number of experimental runs was calculated to be 31 (k=4, x_0=7). The parameters (X_i) were coded as x_i by Eq. (4):

$$x_i=(X_i-X_0)/\delta X \quad (4)$$

where X_0 and δX are the values of X_i at the center point and the step change, respectively [18,26,28]. The ranges and levels of the operational parameters are given in Table 2. The relationship between the input variables and response (color removal (%)) can be described by Eq. (5).

$$Y=\beta_0+\sum_{i=1}^{k}\beta_i x_i+\sum_{i=1}^{k}\beta_{ii}x_i^2+\sum_{i=1}^{k}\sum_{i\neq j=1}^{k}\beta_{ij}x_{ij}+\varepsilon \quad (5)$$

where y is the response, β_0 is the constant response when all factors are set at the medium level (center point), β_i is the linear coefficient, β_{ii} represents the quadratic coefficient, β_{ij} is the interaction coefficient, x_i is the coded variable level, k is the number of independent variables and ε is the residual term [8,23,29]. The least square method was used for calculating the model coefficients through Eq. (5) using Design-Expert package (version 7.0.0). To evaluate the goodness of the CCD model, ANOVA statistics (R^2, adjusted R^2, *F*-test and *t*-test), normal plots and residuals analysis were used. The significance of the regression coefficients was tested by *F* and Student's *t* tests at a 95% confidence level.

Table 2. Ranges and levels of experimental parameters

Factor	Ranges and levels				
	−2	−1	0	+1	+2
$[Dye]_0$ (mg/L) (X_1)	20	30	40	50	60
Sonication time (min) (X_2)	4	8	12	16	20
Adsorbent dosage (g/L) (X_3)	0.45	0.55	0.65	0.75	0.85
Temperature (°C) (X_4)	20	25	30	35	40

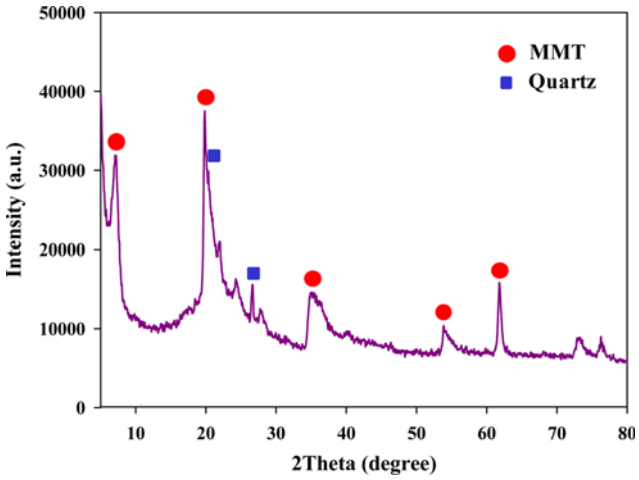

Fig. 1. XRD pattern of the modified nanoclay.

RESULTS AND DISCUSSION

1. Results of Surficial Characterization

1-1. X-ray Diffraction Analysis

The X-ray diffraction (XRD) pattern of the modified nanoclay can be seen in Fig. 1. From the peak positions of the XRD pattern, the basal spacing of the modified nanoclay was obtained. The modified nanoclay shows the characteristic peak of the montmorillonite at 2θ=7.08°, corresponding to the interlayer distance (d_{001}) of 1.2 nm. Moreover, the montmorillonite represented the diffraction peak at 2θ of 7.08°, 19.83°, 35.10°, 54.21° and 61.80°, as well as the quartz at 2θ of 20.8° and 26.6°. These made the dominant phase of the modified nanoclay, thereby indicating the XRD pattern of the as-prepared nanoclay. The average crystal size of the modified nanoclay was quantitatively assessed using Debye-Scherrer equation $d=(k\lambda/\beta\cos\theta)$, where d is the crystal size (nm), k is the Debye-Scherrer constant (0.9), λ is the X-ray wavelength (0.15406 nm), β is the width of the peak with the maximum intensity in half height and θ is the diffraction angle [30]. By using Debye-Scherrer equation, the average crystal size for the interlayer spacing of the modified nanoclay was obtained to be 14.3 nm.

1-2. BET Results

Fig. 2 shows the N_2 adsorption-desorption isotherm and the pore size distribution plot of the modified nanoclay. The BET surface area of the modified nanoclay was determined at 77 K. As shown in (Fig. 2(a)), the adsorbent particles had an isotherm of type IV because hysteresis occurred during the desorption branches, according to the IUPAC classification [31]. The isotherm of the modified nanoclay (Fig. 2(a)) presented a type-H3 hysteresis loop. There was no limiting adsorption at high (P/P_0), probably due to the aggregates (loose assemblages) of plate-like particles forming slit-shaped pores with non-uniform size and/or shape and wide mouths [32]; also, capillary condensation took place in mesopores [33]. It was understood from the isotherm graph that the hysteresis loop appeared at a high pressure range (nearly $P/P^0>0.5$) while adsorption and desorption lines overlapped completely in the low relative pressure range, thereby indicating the presence of ink-bottle type of pores [34]. According to Juang [34], such ink-bottle pores have

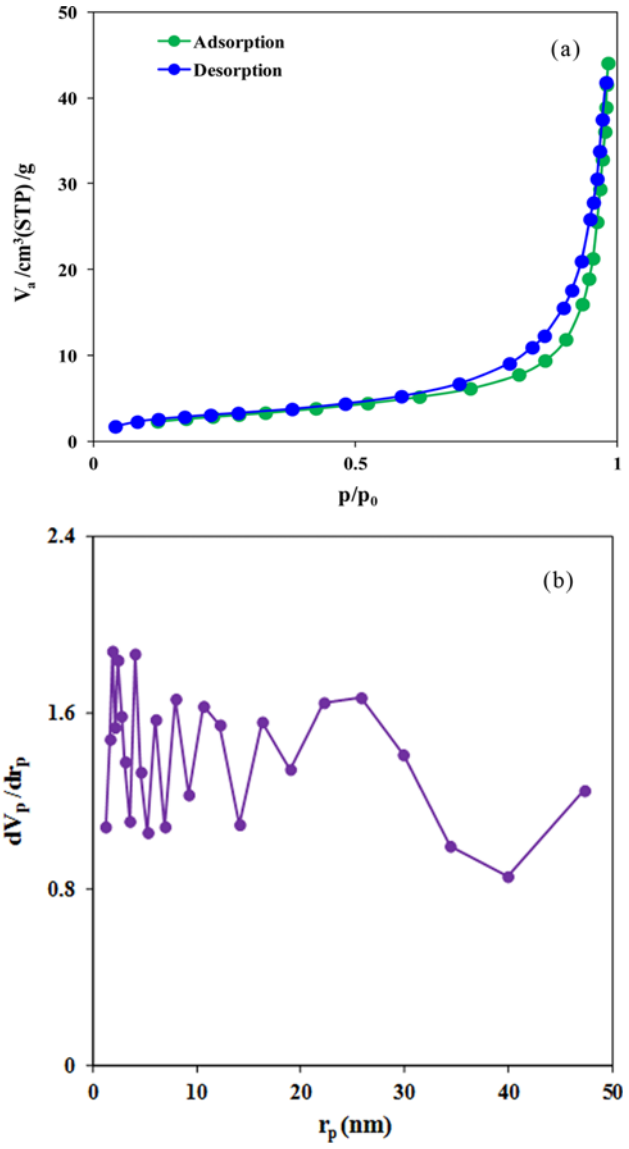

Fig. 2. N_2 adsorption-desorption isotherm of the modified nanoclay (a) and BJH pore size distribution plot (b).

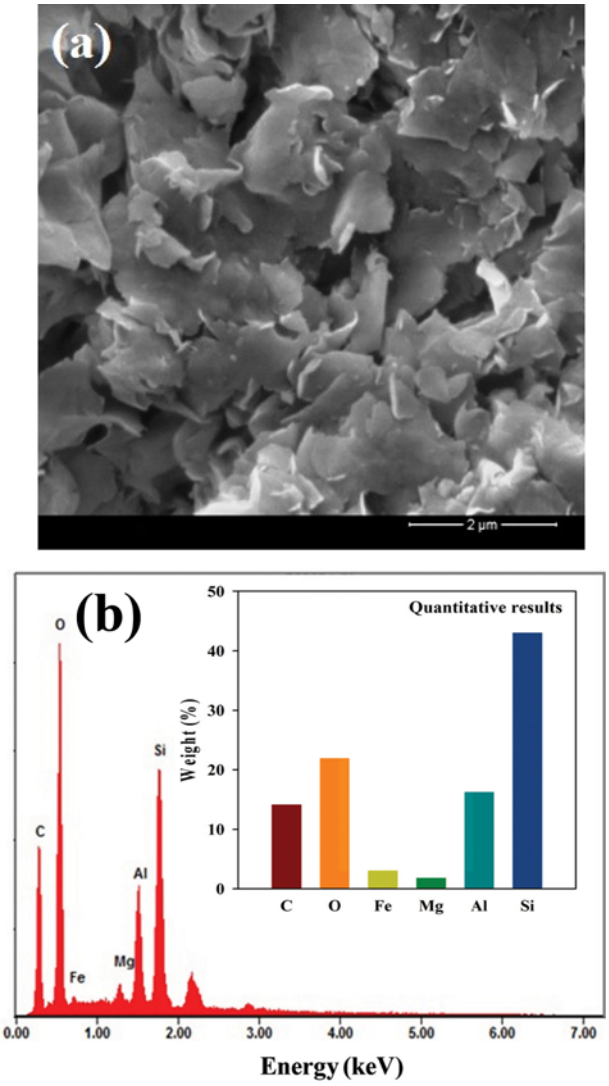

Fig. 3. Scanning electron microscopy image of modified nanoclay surface (a) and EDX analysis with inset displaying weight percent of elements (b).

a large pore diameter since hysteresis occurs at high relative pressures (P/P_0). The extremely lower amounts of nitrogen adsorbed at low relative pressures could indicate the presence of predominant mesopores in the adsorbent structure, because the adsorption capacity in the microporous solids is known to be higher than that of the mesoporous solids. Fig. 2(b) gives the pore size distributions calculated by the BJH method. The calculated surface area and monolayer adsorption capacity of the modified nanoclay [35], as found by the BET equation, were 9.8789 m^2/g and 2.2697 cm^3/g, respectively. The total pore volume and the mean pore diameter were found to be 0.0681 cm^3/g and 27.597 nm, respectively. The BET surface area and the total pore volume of the adsorbent are indicative of the non-uniform textural and the predominantly mesoporous structure of the modified nanoclay (Fig. 2(b)).

1-3. SEM Results

To characterize the surface morphology of the adsorbent, we performed SEM analysis. The results are provided in Fig. 3(a). As is obvious, the adsorbent had a heterogeneous porous and a rough surface; thus, there was a good possibility for the dye molecules to be absorbed via diffusion into the porous structure of the modified nanoclay. Furthermore, the composition of the modified nanoclay was evaluated by EDX analysis, as shown in (Fig. 3(b)). Based on the EDX micrograph, the major portion of the modified nanoclay was composed of Si and O compounds, which were suitable for the interactions between Si-OH groups of the adsorbent and oxygen containing groups of the dye molecules by forming hydrogen bonds in the dyes/water adsorption system. The weight percent (wt%) of Si, O, Al, C, Fe and Mg compounds within the adsorbent was 43.01, 21.89, 16.20, 14.09, 3.02 and 1.78%, respectively.

1-4. FT-IR Results

FT-IR spectra of the modified nanoclay were recorded before and after the adsorption of AO7 and AR17 in a wavenumber ranging from 400 to 4,000 cm^{-1} (Fig. 4). To interpret the FT-IR spec-

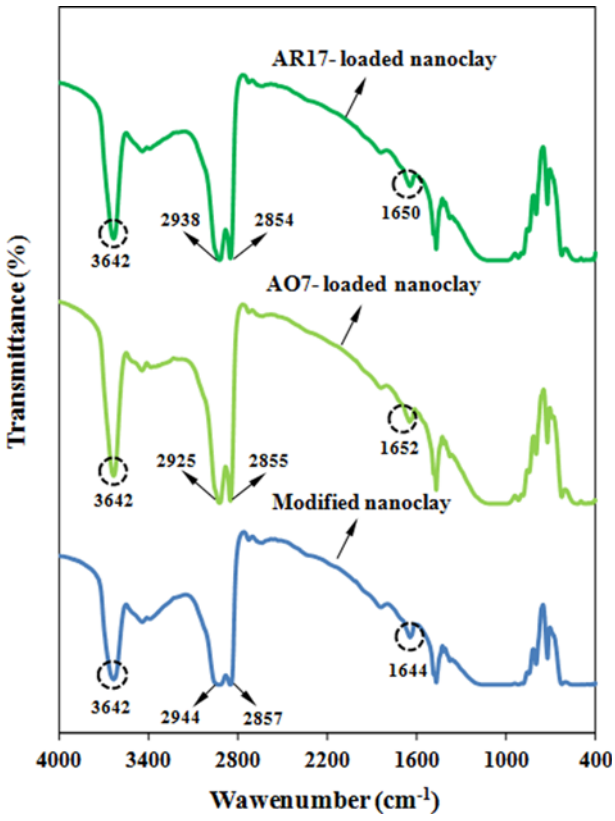

Fig. 4. FT-IR spectrum of the modified nanoclay before and after adsorption of AO7 and AR17 at optimum conditions.

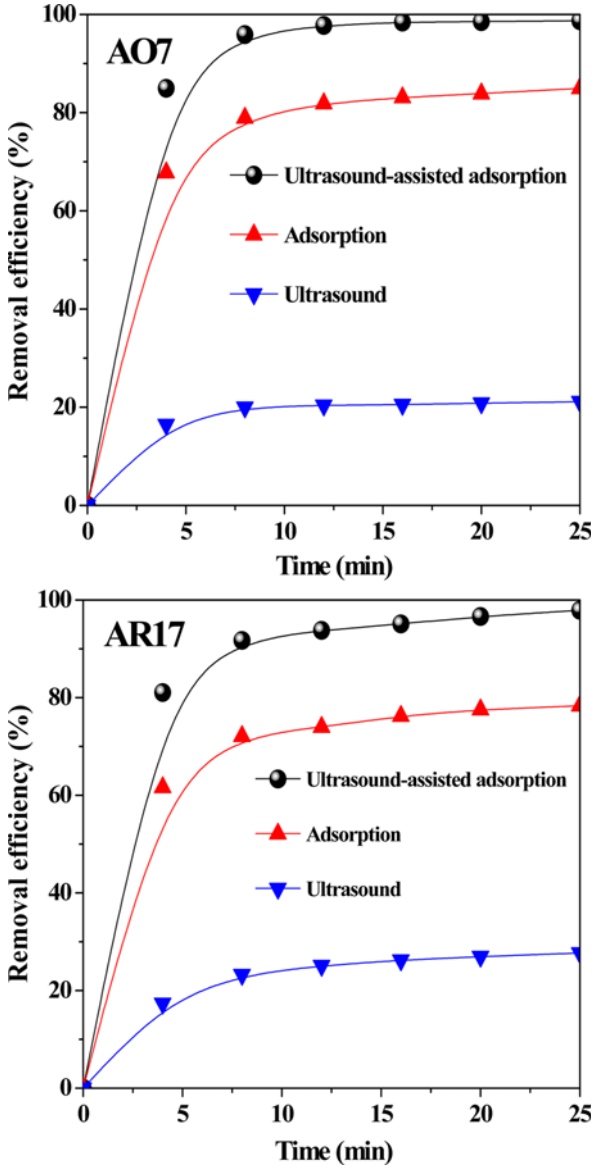

Fig. 5. Comparison of different processes involved in the ultrasound-assisted adsorption of AO7 and AR17 dyes.

tra, the absorption peaks were compared with the standard FT-IR patterns [36-39]. The asymmetric stretching band of the structural OH groups of the modified nanoclay sample appeared at 3,642 cm^{-1} [13,36,40]. The position of this band was not changed after the adsorption of AO7 and AR17, while its transmittance (%) was increased from 32.96% to 61.91% and 52.29% for AO7 and AR17, respectively. It could be demonstrated that the adsorption of AO7 onto the modified nanoclay was stronger than that of AR17 dye. The peaks at 2,944 and 2,857 cm^{-1} corresponded to the -CH_2 asymmetric and -CH_2 symmetric stretching vibrations [36-38]. The shift in these peaks reflected the effective role of these bonds in the adsorption of AO7 and AR17 via electrostatic interactions between the adsorbent surface and the negatively charged dyes. The shift in the wavenumber of H-O-H bending vibration at 1,644 cm^{-1} supported the formation of H-bonds as a proposed mechanism for the adsorption of dye molecules [36,37]. The wavenumber of this band was increased from 1,644 cm^{-1} to 1,652 cm^{-1} and 1,650 cm^{-1} for AO7 and AR17, respectively (Fig. 4). Most of the peaks in the range between 400 and 1,100 cm^{-1} could be assigned to the clay minerals and silicon-containing groups [36]. The FT-IR spectra of the modified nanoclay were observed as a broad peak in a range between 879 and 1,118 cm^{-1}, corresponding to the stretching and bending vibrations of Si-O-Al, Si-O-Si, Al-OH-Al and Al-OH-Mg groups [36,37]. They broadened considerably in the spectra of the dye-loaded modified nanoclay. It could be attributed to the alteration of silica and alumina layers due to the presence of organic chains causing the intercalation of the dye molecules [39]. The shift of bands belonging to Si-O and all -OH vibrations and/or the change in their intensities implied the presence of strong electrostatic interactions and, also, the hydrogen bonds between dye molecules and these functional groups. The -OH group can play a significant role in the adsorption of dye molecules via hydrogen bonding.

2. Comparative Study

Before conducting the systematized experiments for the adsorption of the studied organic dyes onto the modified nanoclay, a comparative study was performed to specify the role of each process in the ultrasound-assisted adsorption of the organic dyes. Fig. 5(a) shows that sonication alone, adsorption alone and ultrasound-assisted adsorption led to AO7 removal efficiency of 21.14, 85.29 and 98.71%, respectively. For the removal of AR17, the sonication alone, adsorption alone and ultrasound-assisted adsorption resulted in AR17 removal efficiency of 31.94, 80.16 and 97.91%, respectively

(Fig. 5(b)). Thus, ultrasound-assisted adsorption can be considered as a selective process for the removal of the studied organic dyes due to its higher removal efficiency as compared to sonication and adsorption alone.

3. CCD Results

The individual and interactive effects of independent variables, including the initial dye concentration, adsorbent dosage, temperature and sonication time, on the color removal (as response) were investigated using CCD approach. A quadratic polynomial model was obtained to characterize the mathematical relationship between the response and independent variables. The observed (experimental) and predicted color removal values (%) for both AO7 and AR17 dyes are presented in Table 3. The empirical relationship between the response and independent variables for the adsorption of AO7 and AR17 is shown in Eqs. (6) and (7):

$$Y(AO7)=65.5577-7.8297x_1+1.9135x_2+3.7431x_3+1.4643x_4+2.4482x_1^2 - 1.1231x_2^2+0.2094x_3^2-0.7211x_4^2+0.1509x_1x_2-0.2175x_1x_3 - 2.0085x_1x_4+3.0983x_2x_3+1.7555x_2x_4+1.8865x_3x_4 \quad (6)$$

$$Y(AR17)=76.4700-8.3724x_1+1.6789x_2+1.9711x_3 +2.9029x_4-2.6552x_1^2-1.6257x_2^2-2.1816x_3^2-6.0625x_4^2 -0.5315x_1x_2+1.2912x_1x_3+1.6739x_1x_4-1.1197x_2x_3 +1.5925x_2x_4-1.7573\ x_3x_4 \quad (7)$$

Determining the interactive effects of different variables along with the prediction of the optimum values of the variables within the specified ranges for the maximum color removal (%) can be done by Eqs. (6) and (7). The statistical significance of the CCD model was assessed by the analysis of variance (ANOVA) [26,29]. The results of ANOVA are summarized in Table 4. The results revealed that the applied model could be successfully used to navigate the design space. According to the data given in Table 4, high values of correlation coefficients (R^2=0.959 for AO7 and R^2=0.971 for AR17) between the predicted and experimental color removal (%) were

Table 3. The 4-factor central composite design matrix and the value of the response function (CR (%))

Run	$[Dye]_0$ (mg/L)	Sonication time (min)	Adsorbent dosage (g/L)	Temperature (°C)	Removal efficiency (%)			
					AO7		AR17	
					Exp.	Pred.	Exp.	Pred.
1	50	8	0.75	25	58.51	57.3	56.67	57.58
2	40	12	0.65	30	65.41	65.55	77.00	76.47
3	40	12	0.65	30	65.38	65.55	79.33	76.47
4	30	8	0.75	25	71.07	69.69	75.15	74.02
5	40	12	0.45	30	57.77	58.90	62.84	63.80
6	50	16	0.75	35	68.31	70.32	64.11	63.27
7	40	12	0.65	30	66.07	65.55	77.12	76.47
8	30	16	0.75	35	90.55	90.13	72.63	75.15
9	40	12	0.65	30	65.67	65.55	75.02	76.47
10	30	8	0.75	35	79.91	76.90	71.08	69.78
11	20	12	0.65	30	87.08	91.01	82.38	82.59
12	60	12	0.65	30	59.67	59.69	48.27	49.10
13	50	8	0.55	25	62.13	60.23	48.18	45.30
14	40	4	0.65	30	52.80	57.23	67.55	66.60
15	30	16	0.55	25	66.21	65.56	73.13	70.38
16	50	16	0.55	25	53.28	54.65	46.02	46.65
17	30	16	0.75	25	77.84	75.90	73.41	73.02
18	30	8	0.55	35	71.73	71.40	66.70	69.70
19	50	8	0.75	35	58.14	56.49	57.65	60.03
20	40	12	0.65	40	65.34	65.60	60.87	58.02
21	40	20	0.65	30	65.37	64.89	71.33	73.32
22	40	12	0.85	30	71.06	73.88	71.59	71.68
23	40	12	0.65	30	64.74	65.55	75.20	76.47
24	40	12	0.65	20	56.05	59.74	42.52	46.41
25	30	8	0.55	25	75.39	71.74	66.74	66.91
26	50	8	0.55	35	51.56	51.86	55.06	54.78
27	40	12	0.65	30	65.59	65.55	76.80	76.47
28	30	16	0.55	35	72.68	72.24	81.12	79.54
29	50	16	0.75	25	66.12	64.13	57.81	54.45
30	40	12	0.65	30	66.01	65.55	74.79	76.47
31	50	16	0.55	35	54.24	53.30	61.74	62.50

Table 4. Analysis of variance (ANOVA) for response surface quadratic models

Source	Degree of freedom	AO7			AR17		
		Sum of squares	F-value	P-value	Sum of squares	F-value	P-value
Model	14	2520.86	26.95	0.000	3465.31	38.99	0.000
Residuals	16	106.91			101.58		
Total	30	2627.77			3566.89		

AO7: R^2=0.959. Adjusted R^2=0.923
AR17: R^2=0.971. Adjusted R^2=0.946

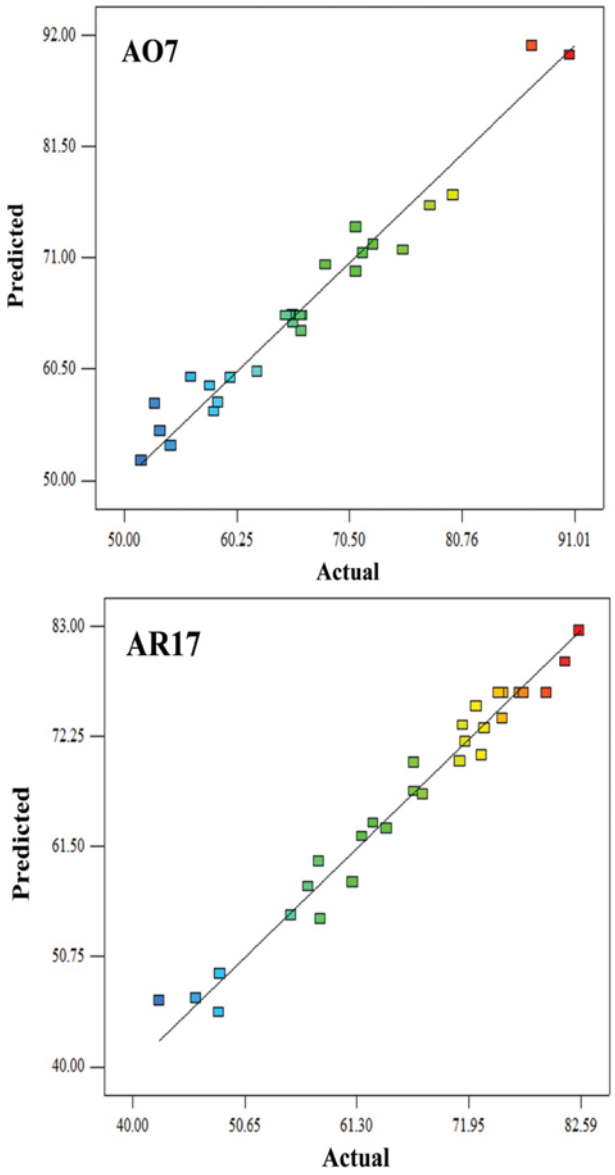

Fig. 6. Comparison of the experimental results of color removal with predicted values by CCD model.

obtained, thereby indicating that the applied model could be reliable for predicting color removal (%). The plots of predicted color removal (%) versus experimental color removal (%) are depicted in Fig. 6, for both AO7 and AR17. They exhibit a good agreement between the predicted and experimental color removal (%). In the case of AO7, the obtained value of 0.959 indicates that 95.9% of the variations for color removal could be explained by the model and the model did not account for only 4.1% of the variations. In the case of AR17, the obtained value of 0.971 shows that 97.1% of the variations could be explained by the model and the model did not account for only 2.9% of the variations. Additionally, it is known that the value of adjusted R^2 adjusts the value of R^2 in terms of the sample size and the number of variables and statistical terms based on the degrees of freedom [29,41,42]. In a system with various independent variables, the adjusted R^2 is more suitable for evaluating the goodness of the applied model. The adjusted R^2 for AO7 (0.923) and the adjusted R^2 for AR17 (0.946) were very close to the corresponding R^2 values, suggesting a good fitness between the predicted and experimental color removal (%). Having many terms in the applied model along with a not very large sample size leads to a smaller adjusted R^2 [43]. The significance of the model was also verified by the obtained F-value and P-value. The larger the quantity of the F-value and smaller the P-value, the more significant was the applied model. The obtained F-value for AO7 and AR17 was 26.95 and 38.99, respectively. The obtained F-value for both AO7 and AR17 was much higher than the Fisher's F-value (2.37 at 95% confidence level), indicating the suitability and adequacy of the model in describing the adsorption of anionic dyes onto the modified nanoclay (Table 4). In addition, evaluation of the residuals could be an appropriate tool to exhibit how well the model satisfied the assumptions of the ANOVA [17,23,26]. This analysis consisted of identifying the outliers and examining the diagnostic plots such as normal probability and residual plots. Normal probability plots could indicate whether the residuals followed a normal distribution or not [44]. Besides, the Pareto analysis could give more significant information to interpret the results of response surficial modeling. In fact, this analysis could calculate the percentage effect of each factor on the response (color removal (%)) as shown in Eq. (8) [43,45,46]:

$$P_i=\left(\frac{b_i^2}{\sum b_i^2}\right)\times 100 \ (i\neq 0) \quad (8)$$

According to the Pareto analysis of AO7 and AR17, the initial dye concentration (56.09% for AO7 and 47.34% for AR17) produced the main effect on the ultrasound-assisted adsorption of both AO7 and AR17.

4. Significance of the Regression Coefficients

The regression coefficient values, standard error, calculated t and F values and significance levels are presented in Table 5. Linear coefficients b_1 and b_3, quadratic coefficient b_{11} and interaction co-

Table 5. Estimated coefficients and their corresponding *F.* t and *P*-values

Term	Coefficient estimate		Standard error		F-value		Student *t*		P-value	
	AO7	AR17	AO7	AR17	AO7	AR17	AO7	AR17	AO7	AR17
b_0	65.5577	76.4700	0.9770	0.9523	-	-	67.100	80.297	0.000	0.000
b_1	−7.8297	−8.3724	0.5276	0.5143	220.20	264.99	−14.839	−16.279	0.000	0.000
b_2	1.9135	1.6789	0.5276	0.5143	13.15	10.66	3.626	3.264	0.002	0.005
b_3	3.7431	1.9711	0.5276	0.5143	50.33	14.69	7.094	3.832	0.000	0.001
b_4	1.4643	2.9029	0.5276	0.5143	7.70	31.86	2.775	5.644	0.014	0.000
b_{11}	2.4482	−2.6552	0.4834	0.4712	25.65	31.76	5.065	−5.635	0.000	0.000
b_{22}	−1.1231	−1.6257	0.4834	0.4712	5.40	11.90	−2.323	−3.450	0.034	0.003
b_{33}	0.2094	−2.1816	0.4834	0.4712	0.19	21.44	0.433	−4.630	0.671	0.000
b_{44}	−0.7211	−6.0625	0.4834	0.4712	2.23	165.55	−1.492	−12.866	0.155	0.000
b_{12}	0.1509	−0.5315	0.6462	0.6299	0.05	0.71	0.234	−0.844	0.818	0.411
b_{13}	−0.2175	1.2912	0.6462	0.6299	0.11	4.20	−0.337	2.050	0.741	0.057
b_{14}	−2.0085	1.6739	0.6462	0.6299	9.66	7.06	−3.108	2.657	0.007	0.017
b_{23}	3.0983	−1.1197	0.6462	0.6299	22.99	3.16	4.794	−1.778	0.000	0.094
b_{24}	1.7555	1.5925	0.6462	0.6299	7.38	6.39	2.717	2.528	0.015	0.022
b_{34}	1.8856	−1.7573	0.6462	0.6299	8.51	7.78	2.918	−2.790	0.010	0.013

efficient b_{23} for AO7 were significant at a confidence level of 95%. Therefore, statistically significant parameters were the linear effect of the initial dye concentration and the adsorbent dosage, the quadratic effect of the initial dye concentration and the interaction effect of sonication time and adsorbent dosage. In the case of AR17, the linear effect of the initial dye concentration and the quadratic effect of temperature were significant at the same confidence level.

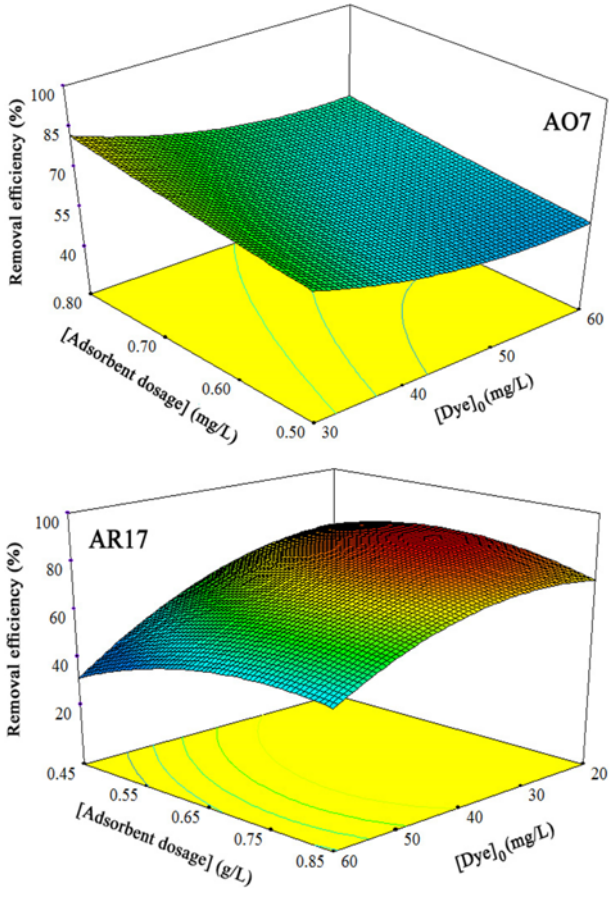

Fig. 7. The response surface of the color removal efficiency (%) as a function of dye initial concentration and adsorbent dosage (temperature=30 °C and sonication time=12 min).

5. The Effect of Operational Parameters

To analyze the interactive effect of the studied operational parameters on the adsorption of AO7 and AR17, three dimensional (3D) and their corresponding contour plots were depicted based on the polynomial function model. The response surface plots (3-D) and their corresponding contour plots could be beneficial in understanding the interactive effects of the selected independent variables [17]. Response surface plots could provide an approach to predict color removal (%) for different values of the tested variables, and contours plots, in turn, could help to identify the type of interactions between the studied variables. Fig. 7 represents the response surface plot as a function of the initial dye concentration and the adsorbent dosage while the sonication time and temperature were kept constant at 12 min and 30 °C, respectively. As can be seen, the color removal efficiency decreased with increasing initial dye concentration. The lower color removal (%) at higher dye concentrations could be attributed to the saturation of the adsorptive sites of the adsorbent [17]. On the other hand, the increase in color removal (%) with decreasing the initial dye concentrations indicates that the adsorption of both AO7 and AR17 was dependent on their initial concentrations. Moreover, Fig. 7 shows the interactive effect of the initial dye concentration and the adsorbent dosage on the color removal (%), where sonication time and temperature were constant at 12 min and 30 °C, respectively. As shown, increasing adsorbent dosage resulted in a sharp increase in color removal (%), indicating that the adsorbent dosage produced a major effect on color removal (%) for both AO7 and AR17. This could be confirmed by the obtained F-value of the adsorbent dosage (Table 5). Increasing adsorbent dosage gave more surface area and subsequently, more binding sites for the adsorption of target pollutants

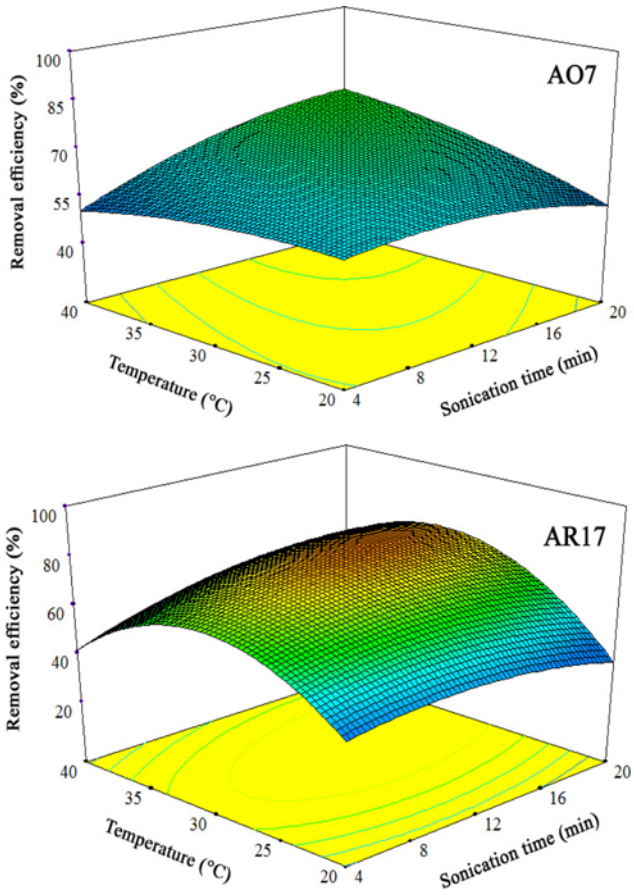

Fig. 8. The response surface of the color removal efficiency (%) as a function of sonication time and temperature (Dye=40 mg/L and adsorbent dosage=0.65 g/L).

onto the modified nanoclay [47]. The interactive effect of sonication time and temperature is shown in Fig. 8. As can be seen, first, increasing the sonication time resulted in a slight increase in the color removal (%), while increasing the sonication time to a specified value caused a little decrease in color removal (%). The increase in the color removal (%) with increasing the sonication time could be attributed to the relatively higher mass transfer and the higher surface area produced by the cavitation process. Decreasing the color removal (%) after a specified sonication time could be a result of the enhanced desorption phenomenon due to the excessive ultrasonication. Anyway, sonication time produced a smaller effect on the adsorption of AO7 and AR17 in comparison with the initial dye concentration. In addition, the color removal (%) was increased with increasing the temperature up to 35 °C, and then decreased (Fig. 8). The increase can be because the adsorption of the studied organic dyes onto the modified nanoclay is endothermic [20]. Increasing color removal (%) with increasing temperature could be attributed to the increasing diffusion rate of dye molecules into the pores and the easy formation of cavitating bubbles due to decreasing the viscosity of the solution, which led to the creation of some new active sites. The decrease in dye removal (%) after 35 °C could be as a result of the less preferable adsorption, with the the tendency of weakly bound dye molecules to escape from adsorbent surface to the solution phase at high temperatures.

Table 6. Obtained optimum values of operational parameters for maximal color removal

Variable	Optimum value	
	AO7	AR17
$[Dye]_0$ (mg/L)	20	30
Sonication time (min)	20	12
Adsorbent dosage (g/L)	0.54	0.65
Temperature (°C)	40	30
Removal efficiency (%) (pred.)	89.99	82.18
Removal efficiency (%) (exp.)	89.31	82.13

6. Optimization

To reach the optimized values of the operational variables for the maximum color removal (%), a numerical optimization was used in which the color removal (%) was set to "maximize" and the operational variables were set to "in range." The results of numerical optimization for the adsorption of both AO7 and AR17 onto the modified nanoclay are provided in Table 6. The results of numerical optimization for AO7 showed that a maximum color removal (%) of 89.99% could be achievable with an initial AO7 concentration of 20 mg/L, adsorbent dosage of 0.54 g/L, sonication time of 20 min and temperature of 40 °C. For AR17, maximum color removal (%) of 82.18% could be achievable with the initial AR17 concentration of 30 mg/L, the adsorbent dosage of 0.65 g/L, the sonication time of 12 min and the temperature of 30 °C. In the following,

Table 7. Comparison of the removal efficiency of various adsorbents for the removal of dyes

No.	Adsorbent	Adsorbate	BET surface area (m^2/g)	Removal efficiency (%)	Ref.
1	Organoclay	Malachite Green	9.3	99.60	[16]
2	CTAB-MBn	Congo Red	18.41	99.94	[48]
3	Activated clay	Methylene Blue	10.1	95.00	[49]
4	Kaolin	Brilliant Green	13.69	98.00	[50]
5	Chi-MMT	Basic Blue 9	23	97.00	[51]
6	Chi-MMT	Basic Blue 66	23	99.00	[51]
7	Chi-MMT	Basic Yellow1	23	92.00	[51]
8	Modified nanoclay	Acid Orange 7	9.87	89.31	This work
9	Modified nanoclay	Acid Red 17	9.87	82.13	This work

confirmatory experiments were carried out under optimized values to verify the results of numerical optimization. The experimental color removal (%) for AO7 and AR17 was found to be 89.31% and 82.13% under optimum operational parameters, respectively. This indicated the reliability of the applied model for the estimation of the real conditions. The removal efficiency of various natural and modified clays as the potential adsorbent for the removal of dyes is shown in Table 7. As depicted, the removal efficiency of the modified nanoclay was comparable to that of the other listed adsorbents [16,48-51]. Therefore, the modified nanoclay can be considered as an effective adsorbent for treating the colored solutions.

7. Possible Adsorption Mechanism

Natural modified nanoclay particles have a very high positive surface charge at natural pH (+74.5 mV), probably due to the presence of dispersive interactions between parts of alkyl groups of the adsorbed $R_1R_2(CH_3)_2N^+$ ions in the basal space of montmorillonite and attached $R_1R_2(CH_3)_2N^+$ ions which are partly horizontal [52]. According to this, it can be stated that various interactions are effective in the adsorption mechanism. One of them refers to the electrostatic interactions between positively charged functional groups on the modified nanoclay surface and ions of and that come from the dye molecules. The second mechanism involves hydrogen bonds, which carry out Si-OH and Al-OH groups of the adsorbent and oxygen containing groups of the dye molecules. Also, there is the probability of hydrophobic interaction between alkyl groups of the modified nanoclay and dye molecules.

CONCLUSION

Response surface methodology based on central composite design was applied to optimize the operational parameters for the maximum ultrasound-assisted adsorption of textile dyes onto the modified nanoclay. The results of ANOVA showed that CCD model could be an efficient approach for the optimization of the experimental variables. The results of Pareto analysis also showed that the initial dye concentration had a significant effect on the color removal. Furthermore, the results of FT-IR analysis confirmed the involvement of O-H and N-H groups in dyes and modified nanoclay interaction. It can be, therefore, concluded that the commercial modified nanoclay is an efficient adsorbent for the removal of two textile dyes via ultrasound-assisted adsorption.

ACKNOWLEDGEMENTS

The authors would like to thank the Atatürk University of Erzurum (Turkey) and University of Tabriz (Iran) for the support provided.

REFERENCES

1. A. R. Khataee, F. Vafaei and M. Jannatkhah, *Int. Biodeter. Biodegr.*, **83**, 33 (2013).
2. M. Roosta, M. Ghaedi, A. Daneshfar and R. Sahraei, *Spectrochim. Acta A*, **122**, 223 (2014).
3. G. Kiani, M. Dostali, A. Rostami and A. R. Khataee, *Appl. Clay Sci.*, **54**, 34 (2011).
4. M. Shirmardi, A. Mahvi, B. Hashemzadeh, A. Naeimabadi, G. Hassani and M. Niri, *Korean J. Chem. Eng.*, **30**, 1603 (2013).
5. A. Gürses, A. Hassani, M. Kıranşan, Ö. Açışlı and S. Karaca, *J. Water Process Eng.*, **2**, 10 (2014).
6. S. Karaca, A. Gürses, Ö. Açışlı, A. Hassani, M. Kıranşan and K. Yıkılmaz, *Desalin. Water Treat.*, **51**, 2726 (2013).
7. Z. Noorimotlagh, R. Darvishi Cheshmeh Soltani, A. R. Khataee, S. Shahriyar and H. Nourmoradi, *J. Taiwan Inst. Chem. Eng.*, **45**, 1783 (2014).
8. A. Hassani, L. Alidokht, A. R. Khataee and S. Karaca, *J. Taiwan Inst. Chem. Eng.*, **45**, 1597 (2014).
9. M. Kıranşan, R. Darvishi Cheshmeh Soltani, A. Hassani, S. Karaca and A. Khataee, *J. Taiwan Inst. Chem. Eng.*, **45**, 2565 (2014).
10. R. Darvishi Cheshmeh Soltani, A. R. Khataee, M. Safari and S. W. Joo, *Int. Biodeter. Biodegr.*, **85**, 383 (2013).
11. A. Khataee, L. Alidokht, A. Hassani and S. Karaca, *Adv. Environ. Res.*, **2**, 291 (2013).
12. R. Darvishi Cheshmeh Soltani, G. S. Khorramabadi, A. R. Khataee and S. Jorfi, *J. Taiwan Inst. Chem. Eng.*, **45**, 973 (2014).
13. G. Shams Khorramabadi, R. Darvishi Cheshmeh Soltani, A. Rezaee, A. R. Khataee and A. Jonidi Jafari, *Can. J. Chem. Eng.*, **90**, 1539 (2012).
14. R. Lafi, A. ben Fradj, A. Hafiane and B. H. Hameed, *Korean J. Chem. Eng.*, **31**, 2198 (2014).
15. Y. Park, G. A. Ayoko and R. L. Frost, *J. Colloid Interface Sci.*, **354**, 292 (2011).
16. S. Arellano-Cárdenas, S. López-Cortez, M. Cornejo-Mazón and J. C. Mares-Gutiérrez, *Appl. Surf. Sci.*, **280**, 74 (2013).
17. R. Darvishi Cheshmeh Soltani, A. Khataee, H. Godini, M. Safari, M. Ghanadzadeh and M. Rajaei, *Desalin. Water Treat.*, 1 (2014).
18. A. Hassani, R. Darvishi Cheshmeh Soltani, S. Karaca and A. Khataee, *J. Ind. Eng. Chem.*, **21**, 1197 (2015).
19. E. Şayan, *Chem. Eng. J.*, **119**, 175 (2006).
20. M. Roosta, M. Ghaedi, N. Shokri, A. Daneshfar, R. Sahraei and A. Asghari, *Spectrochim. Acta A*, **118**, 55 (2014).
21. M. Chaichi, A. Mohammadi and M. Hashemi, *Microchem. J.*, **108**, 46 (2013).
22. P. Sharma, L. Singh and N. Dilbaghi, *J. Hazard. Mater.*, **161**, 1081 (2009).
23. R. Darvishi Cheshmeh Soltani, A. Rezaee, A. R. Khataee and M. Safari, *J. Ind. Eng. Chem.*, **20**, 1861 (2014).
24. R. Darvishi Cheshmeh Soltani, A. Rezaee, H. Godini, A. R. Khataee and A. Hasanbeiki, *Chem. Ecol.*, **29**, 72 (2013).
25. J. P. Silva, S. Sousa, I. Gonçalves, J. J. Porter and S. Ferreira-Dias, *Sep. Purif. Technol.*, **40**, 163 (2004).
26. R. Darvishi Cheshmeh Soltani, A. Rezaee, A. Khataee and H. Godini, *Can. J. Chem. Eng.*, **92**, 13 (2014).
27. R.-L. Tseng and S.-K. Tseng, *J. Hazard. Mater.*, **136**, 671 (2006).
28. F. Mahdizadeh, M. Eskandarian, J. Zabarjadi, A. Ehsani and A. Afshar, *Korean J. Chem. Eng.*, **31**, 74 (2014).
29. A. R. Khataee, M. B. Kasiri and L. Alidokht, *Environ. Technol.*, **32**, 1669 (2011).
30. A. Khataee, M. Sheydaei, A. Hassani, M. Taseidifar and S. Karaca, *Ultrason. Sonochem.*, **22**, 404 (2015).
31. M. J. Rosen, *Surfactants and interfacial phenomena*, John Wiley & Sons, New York (1978).
32. W.-T. Tsai, J.-M. Yang, H.-C. Hsu, C.-M. Lin, K.-Y. Lin and C.-H.

Chiu, *Micropor. Mesopor. Mater.*, **111**, 379 (2008).
33. F. Adam, J. N. Appaturi, R. Thankappan and M. A. M. Nawi, *Appl. Surf. Sci.*, **257**, 811 (2010).
34. R.-S. Juang, F.-C. Wu and R.-L. Tseng, *Colloids Surf., A*, **201**, 191 (2002).
35. S. Brunauer, L. S. Deming, W. E. Deming and E. Teller, *J. Am. Chem. Soc.*, **62**, 1723 (1940).
36. Y. Ma, J. Zhu, H. He, P. Yuan, W. Shen and D. Liu, *Spectrochim. Acta A*, **76**, 122 (2010).
37. W. Xue, H. He, J. Zhu and P. Yuan, *Spectrochim. Acta A*, **67**, 1030 (2007).
38. T. Mandalia and F. Bergaya, *J. Phys. Chem. Solids*, **67**, 836 (2006).
39. E. Onder, N. Sarier, G. Ukuser, M. Ozturk and R. Arat, *Thermochim. Acta*, **566**, 24 (2013).
40. R. Darvishi Cheshmeh Soltani, A. Rezaee and A. Khataee, *Ind. Eng. Chem. Res.*, **52**, 14133 (2013).
41. M. Fathinia, A. R. Khataee, M. Zarei and S. Aber, *J. Mol. Catal. A: Chem.*, **333**, 73 (2010).
42. K. P. Singh, S. Gupta, A. K. Singh and S. Sinha, *J. Hazard. Mater.*, **186**, 1462 (2011).
43. A. R. Khataee, M. Zarei and L. Moradkhannejhad, *Desalination*, **258**, 112 (2010).
44. L. Alidokht, A. R. Khataee, A. Reyhanitabar and S. Oustan, *CLEAN - Soil, Air, Water*, **39**, 633 (2011).
45. A. K. Abdessalem, N. Oturan, N. Bellakhal, M. Dachraoui and M. A. Oturan, *Appl. Catal. B*, **78**, 334 (2008).
46. A. Esfahani, S. Hojati, A. Azimi, L. Alidokht, A. Khataee and M. Farzadian, *Korean J. Chem. Eng.*, **31**, 630 (2014).
47. M. Kousha, E. Daneshvar, M. S. Sohrabi, N. Koutahzadeh and A. R. Khataee, *Int. Biodeter. Biodegr.*, **67**, 56 (2012).
48. A. Ma, Y. Am and M. M. Al-Awadhi, *J. Anal. Bioanal. Technol.*, **4** (2013).
49. C.-H. Weng and Y.-F. Pan, *J. Hazard. Mater.*, **144**, 355 (2007).
50. B. K. Nandi, A. Goswami and M. K. Purkait, *J. Hazard. Mater.*, **161**, 387 (2009).
51. P. Monvisade and P. Siriphannon, *Appl. Clay Sci.*, **42**, 427 (2009).
52. S. Karaca, A. Gürses and M. Ejder Korucu, *J. Chem.*, **2013**, 10 (2013).